ELSEVIER

Thin Solid Films 374 (2000) 311–325

thin solid films

www.elsevier.com/locate/tsf

SiO_2 etching in inductively coupled C_2F_6 plasmas: surface chemistry and two-dimensional simulations

John Feldsien, Doosik Kim, Demetre J. Economou*

Plasma Processing Laboratory, Department of Chemical Engineering, University of Houston, Houston, TX 77204-4792, USA

Received 28 April 2000; accepted 10 May 2000

Abstract

A surface chemistry model was developed to understand the mechanism of etching or deposition on silicon dioxide surfaces exposed to a high density C_2F_6 plasma. The surface chemistry model in combination with a gas phase plasma chemistry model was implemented in the Modular Plasma Reactor Simulator (MPRES) to study oxide etching and uniformity under typical processing conditions. Simulation results on etch rate and uniformity as a function of operating conditions were consistent with experimental data. The transition from polymerization to etching as the ion bombardment energy (bias power) was increased was also captured by the simulation. Under low pressure conditions (several mtorr) the ion flux peaked at the wafer center while the neutral flux peaked at the wafer edge. Under such conditions, the oxide etch rate was highest at the edge. This supports the conclusion that, at such low pressures, oxide etching is ion driven but neutral dominated. © 2000 Elsevier Science S.A. All rights reserved.

Keywords: SiO_2; C_2F_6 plasmas; Polymerization

1. Introduction

Selective etching of silicon dioxide (oxide) over silicon or silicon nitride using fluorocarbon plasmas is widely known [1–6]. Fluorocarbon plasmas tend to produce CF_x radicals that may polymerize on surfaces in contact with the plasma. Oxygen from the oxide surface, aided by ion bombardment, can prevent the buildup of polymer, allowing net etching of oxide. The lack of oxygen, on the other hand, permits polymer deposition on silicon or silicon nitride surfaces, thus promoting selectivity. However, the mechanistic pathways taken to produce either etching or polymer deposition are not well understood at present.

Fluorocarbon chemistries have been studied in capacitively coupled plasma (CCP) [7–10,55], electron cyclotron resonance (ECR) [4,5,11,12], and inductively coupled plasma (ICP) systems [1,2,13,14]. A variety of different diagnostic techniques, including appearance mass spectroscopy (AMS) [2,15], infrared diode laser absorption spectroscopy (IRDLAS) [16,17], laser-induced fluorescence (LIF) [18–20], and vacuum ultraviolet absorption spectroscopy (VUVAS) [21], have been used to examine the species present in these plasmas. In addition, X-ray photoelectron spectroscopy (XPS) has been used to probe the surfaces in contact with fluorocarbon plasmas [2,4,5,10,15].

Several studies have been reported on the surface reaction probabilities for various CF_x radicals. Booth et al. [19], Tserepi et al. [20], and Thomas et al. [22], all used LIF to examine the loss of CF and CF_2 on various surfaces. In addition, IRDLAS has been used by Takahashi et al. [12], to examine the behavior of CF_x radicals in an ECR system. Fluorocarbon radicals have also

* Corresponding author.
E-mail address: economou@uh.edu (D.J. Economou).

0040-6090/00/$ - see front matter © 2000 Elsevier Science S.A. All rights reserved.
PII: S0040-6090(00)01156-1

been studied using AMS by Hikosaka et al. [8,15], Ito et al. [9], and Tserepi et al. [23]. Finally, VUVAS has been used by Sasaki et al. [21], to examine fluorine atoms in a helicon high-density discharge. Unfortunately, neither the reaction products nor the surface reaction pathways are well defined in these studies. Therefore, the reaction coefficient information may be used only as an estimate.

Ions interact with suraces in contact with the plasma with varying degrees of reactivity. Steinbruchel et al. [6], produced evidence that in a non-polymerizing CHF_3/O_2 plasma in a reactive ion etching (RIE) system, ions were the main reactive species in etching oxide. They also suggested that the etch or sputtering yields for different ionic species be used along with knowledge of the ion flux to determine etch rates. This proposal of ion reactivity is corroborated by studies done using mass selected ion beams of known composition [24–29]. In beam studies by Mayer et al. [25,26], and Shibano et al. [29], it was observed that more fluorinated ions have higher yields on both silicon and silicon dioxide substrates. Although more fluorinated ions are more massive and, therefore, may be expected to have larger sputtering yields, there is evidence of a chemical effect due either to the larger amount of fluorine in the CF_2^+ and CF_3^+ ions and/or to reactive adsorbed neutrals on the oxide surface. The only difficulty with using the yield information from any of the above studies is the unknown character of the surfaces undergoing etching. In particular, there is an unknown and uncharacterized flux of neutral radicals which can change the reactivity of the surface through adsorption and bonding of the neutrals to the surface. Even with this weakness, however, such beam studies are useful in understanding oxide etching and selectivity.

In addition to the beam studies, there is a large amount of information dealing with etching in actual plasmas. Of particular interest are studies that employ high-density plasma systems, such as ICP or ECR, in which the bias voltage of the etchable substrate surface may be easily changed independently of the source power. This allows the determination of etch behavior at different ion bombardment energies. This also allows the observation of the onset of polymer film deposition onto surfaces in contact with the plasma when those surfaces are not bombarded with sufficiently energetic ions.

Polymer deposition behavior, including ion assisted deposition, was studied specifically by Gotoh et al. [11] and Fracassi et al. [30]. The transition from net film deposition to net oxide etching was also examined experimentally in several studies in both ECR and ICP systems [1,4,5,14]. Oehrlein et al. studied this regime using CF_4 and CHF_3 chemistries in the two different high-density sources. The oxide etch behavior with both low- and high-density plasmas has been studied by many other authors as well. Low-density capacitively-coupled plasma sources were used to examine etch behavior by both Simko et al. [32], and Steinbruchel et al. [6]. High-density plasma sources were used in oxide etch studies by Ding et al. [33], in which an ECR source was used, and Fukasawa et al. [13] in which an ICP source was used.

Along with the wealth of experimental information, there have been several models proposed in an effort to explain the experimental trends. Ding et al. [34], and Misaka et al. [35], developed surface species concentration models for reactions involving adsorbed species and incoming ions. Han et al. [36], reported a profile evolution model for oxide etching in which a modified sticking coefficient was used to model the interaction between adsorbed species and the surface. Finally, Gray et al. [37], undertook a study of oxide etching in pure fluorine enhanced by argon ions. They postulated a set of chemical and ion enhanced reactions that may take place on the surface of the oxide and created a simple three-parameter model including chemical etching, ion-assisted etching and sputtering. Chemical etching was modeled through an Arrhenius-type expression suggested by Flamm et al. [38,39]. Sputtering was assumed to follow a law based on the square root of energy [4–6,14,37]. Rate coefficient fits to data for this simplified system (no polymer deposition) were quite good.

The purpose of this work is twofold: (a) to develop a model for the surface chemistry of oxide etching in fluorocarbon plasmas; and (b) to implement this model, along with plasma chemical reactions, in a two-dimensional self-consistent plasma reactor simulator (MPRES) to study oxide etch rate and uniformity in an inductively coupled system [49].

2. Surface chemistry model development

2.1. Fluorocarbon etch behavior

Most of the discussion in the literature has centered on the macroscopic behavior of fluorocarbon-containing plasmas, but little has been mentioned about the mechanisms or reactions taking place. By focusing on a few recurring themes, a more detailed model may be derived. The main underlying behavior of fluorocarbon plasmas is their ability to produce reactive radicals and ions (CF_x and CF_x^+). The radicals have a tendency to adsorb onto surfaces exposed to the plasma and, if unchecked, can form polymer films on these surfaces. What is not well known is the mechanism of film deposition. For instance, the radical thought to be most associated with polymer film growth in capacitively-coupled systems is CF_2 [31,32,40], but analysis of the deposited films in both capacitive and inductive systems shows that the [F]/[C] (fluorine to carbon atom con-

centration) ratio of the films is less than 2.0 [2,4,44]. This would, at first, suggest that CF could also play a major role in the film growth. In addition, in high density systems, CF may be one of the most prevalent fluorocarbon radicals [2,12]. Because there is no definite information on the elementary steps involved in either the etch or deposition steps under consideration, the analysis must use the common behavior found to some degree in all the systems discussed in the literature:

1. The oxide etch rate depends on the ion flux and ion energy [4–6,37].
2. Under normal operating conditions using CF_4 or CHF_3 with relatively small amounts of H_2, capacitively-coupled systems (RIE mode) exhibit little to no polymer film build-up on powered (or high-bias) electrode surfaces [6,32].
3. In general, three behavioral regimes have been found as substrate bias voltage (ion energy) is varied (Fig. 1). At low bias (polymer deposition regime), polymer deposition occurs over all surfaces. At mid-range bias (polymer suppression regime), a decrease in the polymerization rate and a transition to etching is observed. At high bias (ion-assisted etching regime), the etch rate increases slowly with substrate bias [4,14].
4. The [F]/[C] ratio in deposited films hovers at approximately 1.0 for most conditions, although high ion bombardment appears to drive the ratio to lower values (which suggests the liberation of fluorine from the films with increased ion bombardment) [4,41].
5. A number of studies have found a steady-state fluorocarbon film on the oxide surface while etching is occurring [4,5,14].

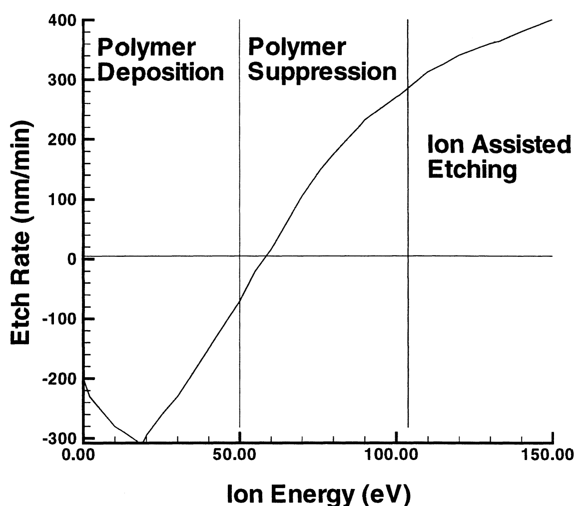

Fig. 1. Example of etch rate vs. ion energy behavior produced by the model. Negative etch rates imply fluorocarbon film deposition. At low ion energies, ion bombardment actually increases the deposition rate.

6. Under some conditions, an enhancement in the polymer film growth rate is seen with increasing ion energy. This enhancement occurs at the low end of the ion energy spectrum and is eventually dominated by polymer etching or sputtering, which drives the polymer film growth rate down at larger ion energies [4,30].
7. The disappearance rates of the three main fluorocarbon radicals have been studied and the sticking coefficient appears to range from low values (0.0001–0.06) for CF_2 and CF_3 to a substantial value (0.1–0.2) for CF [8] [15,19,20,22,23].
8. There appear to be differences in the reactivity of the different fluorocarbon ions with respect to the oxide surface. Etch yields for more fluorinated CF_x^+ ions are greater than for the lesser fluorinated ions (such as CF^+) [24–26,29].

Examining item (1) above, it may be concluded that the oxide etch rate is driven by ions. Any oxide etch mechanism should include a dependence on both the ion flux and ion energy. Looking at items (2) and (3) above, it may be seen that experiments in different systems most likely mirror different parts of the three regimes (Fig. 1) described under item) (3). apacitively coupled reactors, with a large bias voltage across the sheath, would drive the system to the oxide etching regime. From items (1), (3), (4), (5) and (6) above, it may be concluded that the ion energy (r.f. bias) must play a role in determining not only the oxide etching, but also the film growth characteristics. Items (4) and (6) appear to suggest that the ions also play an active role in both the deposition and sputtering behavior of any polymer film that may be present on surfaces in contact with the plasma. In addition, item (5) suggests that there is a difference between the behavior of a thick polymer film and a thin fluorocarbon layer on the surface. It would seem plausible that this difference may appear due to the ability of high energy ions to penetrate and mix a thin fluorocarbon layer with the oxide underneath. This mechanism will not work on a thicker polymer layer because the ions will not be able to penetrate all the way to the oxide/polymer interface. Finally, items (7) and (8) suggest that the chemical nature of both ions and neutrals is important in determining either the etch or deposition behavior seen in the system. To a first degree, species with more fluorine appear to be more reactive, which will provide guidance in choosing reaction rate parameters governing similar reactions for different species.

2.2. Proposed surface chemistry model

Based on this behavior, the following mental picture of an oxide surface exposed to a fluorocarbon plasma emerges, see Fig. 2. Starting from the left, the oxide

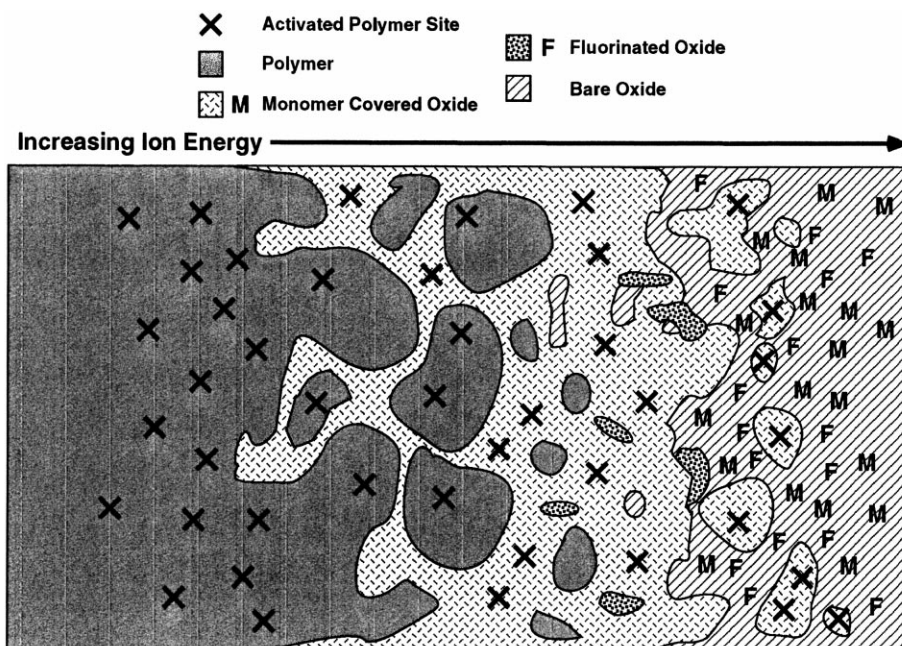

Fig. 2. Visualization of chemical coverages on the oxide surface exposed to a fluorocarbon plasma vs. ion energy (increasing to the right). Coverages include polymer, activated polymer, monomer, and fluorine. As the ion energy becomes very large, bare oxide surface may also be exposed.

surface is bombarded by low-energy ions and a flux of neutral radicals. These radicals will have a tendency to stick or deposit on the surface. If there is insufficient energy provided by the ions to dislodge deposits, a fluorocarbon polymer film will form over the entire surface.

As ion-bombardment energy is increased, ions have enough energy to 'damage' the polymer film, but not enough to significantly sputter or etch the film. These damaged sites on the polymer, shown by X's in Fig. 2, may be thought of as dangling bonds or defluorinated sites in the CF_x network that will be more reactive toward impinging neutral radicals. Adsorption of neutral radicals will occur on these damaged or 'activated' sites at higher rates compared to the surrounding polymer surface, and this will increase the polymer deposition rate.

As ion energy is increased further, ions have enough energy to induce etching or sputtering of the polymer film. Competition now exists between activated deposition and ion-driven etching of the polymer. In Fig. 2, this region is denoted by the break-up of the polymer film, which used to cover the entire surface, and the exposure of thin fluorocarbon (monomer and fluorinated) layers underneath. Continued increase in ion bombardment energy helps in removing the polymer film.

Because the steady-state fluorocarbon film observed on oxide surfaces under etching conditions has a fluorine to carbon atom composition ratio of approximately 1:1 [4,5,14,41], the coverage labeled 'monomer' in Fig. 2 may be thought of as CF adsorbed on the oxide surface. This monomer layer is different from the polymer layer because it bonds to the oxide, as opposed to being bonded only to other CF_x's as in the polymer film. Also, any uncovered oxide surface will have open sites for adsorption of extra fluorine that might be present on an incoming radical (dissociative adsorption). Therefore, if the surface is bombarded or mixed at all, fluorine attached to CF_2 or CF_3 may be stripped from the carbon to fill empty surface sites.

Another type of coverage, found directly on top of the oxide surface, is the fluorinated oxide coverage. Fluorinated sites may be thought of as atomic fluorine bonded or adsorbed to the bare oxide surface. The source of the fluorine may be either fluorocarbon radicals or ions or atomic fluorine from the gas phase. Both monomer and fluorinated coverages are thought to be active in promoting etching with sufficient ion-bombardment energy. The carbon and fluorine atoms in these coverages are used as reactants in the etch reactions. Because of this, increases in ion-bombardment energy lead to depletion of both monomer and fluorinated coverages and the exposure of the bare oxide surface underneath. The regime of high ion bombardment energy is shown near the right hand side of Fig. 2. Sputtering may take place on the bare oxide surface, although ion-assisted etching is favored at the more chemically active fluorinated and monomer covered sites.

It should be noted that the above description, although helpful in visualizing the behavior of the sur-

face under different conditions, does not mirror the exact behavior found in the real system. It is understood that an oxide surface under etching conditions will have a mixed layer of oxide, carbon and fluorine species at the surface. Also, these components may be present in greater than one monolayer of coverage on the oxide, especially in the case of polymer deposition. However, for purposes of generating a model that produces the observed behavior, it does not seem unreasonable to assume that this mixed layer may be represented by thin surface coverages of the components found in the mixed layer, i.e. activated polymer, polymer, monomer, fluorine and oxide (open) site coverages.

The reactions to be taken into account are shown in Table 1. It must be noted that these reactions are not elementary, as this would involve a much larger number of surface species and reaction steps, with a corresponding increase in the number of parameters. For this reason, phenomenological reactions are used so that a smaller number of rate expressions may be dealt with, while still obtaining the correct behavior from the model.

The basic reaction types are as follows: adsorption and polymer growth, polymer activation and sputtering, and oxide ion-assisted etching and chemical sputtering. Reactions R1 and R2 show adsorption of atomic fluorine and fluorocarbon radicals on bare oxide sites. Atomic fluorine and CF are assumed to use single sites on the oxide surface and produce single fluorinated and monomer sites, respectively. The more-fluorinated fluorocarbon radicals (CF_2 and CF_3) use two oxide sites, and free F is released in the gas phase in the case of CF_3. This keeps the stoichiometry of the monomer coverage constant, which allows more consistent balancing of species in the etch reactions.

Table 1
Reactions taken into account in the oxide surface chemistry model[a]

Adsorption and polymer growth

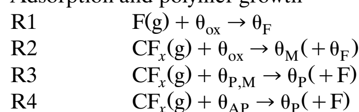

R1	$F(g) + \theta_{ox} \rightarrow \theta_F$
R2	$CF_x(g) + \theta_{ox} \rightarrow \theta_M(+\theta_F)$
R3	$CF_x(g) + \theta_{P,M} \rightarrow \theta_P(+F)$
R4	$CF_x(g) + \theta_{AP} \rightarrow \theta_P(+F)$

Polymer activation and sputtering

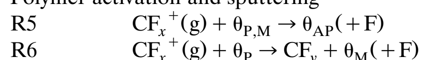

R5	$CF_x^+(g) + \theta_{P,M} \rightarrow \theta_{AP}(+F)$
R6	$CF_x^+(g) + \theta_P \rightarrow CF_y + \theta_M(+F)$

Ion-assisted etching and chemical sputtering

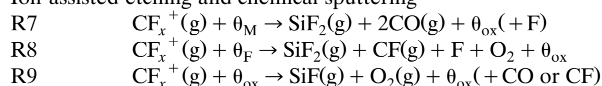

R7	$CF_x^+(g) + \theta_M \rightarrow SiF_2(g) + 2CO(g) + \theta_{ox}(+F)$
R8	$CF_x^+(g) + \theta_F \rightarrow SiF_2(g) + CF(g) + F + O_2 + \theta_{ox}$
R9	$CF_x^+(g) + \theta_{ox} \rightarrow SiF(g) + O_2(g) + \theta_{ox}(+CO \text{ or } CF)$

[a] *Note.* Surface coverages are shown as θ with subscripts: ox, oxide; P, polymer; M, monomer; AP, activated polymer, see also Fig. 2, (g) implies gas phase species. Added species in parenthesis (e.g. +F) imply that corresponding species is liberated when more fluorinated radicals are reacting.

Reactions R3 correspond to growth of polymer on existing polymer or fluorocarbon (monomer) coverage on the surface, while R4 accounts for polymer growth on activated polymer sites. This is done by accounting for the disappearance of the CF_x radicals from the gas phase near the surface and using this disappearance rate to produce a deposition rate of polymer on the surface. In the case of deposition on the polymer (or activated polymer) surface, this occurs without any change in the values of the site densities. In this way, the deposition of more than one monolayer of adsorbates on the oxide may be taken into account. On the monomer-covered surface, deposition produces a polymer film and therefore the reactions are written to produce the polymer coverage. The production of gaseous fluorine by reactions R3 and R4 is assumed in order to keep the fluorine to carbon concentration ratio of the depositing film at reasonable levels (between 1 and 2 for films depositing without excessive ion bombardment). This range is experimentally seen in studies using XPS to probe surfaces exposed to fluorocarbon plasmas [2,4,40].

Reactions R5 depict the ion-assisted activation of polymer or monomer surfaces. Ion bombardment has the effect of defluorinating the polymer and so these reactions have been written to include the liberation of atomic fluorine to the gas phase. Etching of polymer is shown in reactions R6. Etching, like polymer activation, is also ion driven. The polymer etch reactions produce the underlying monomer coverage on the surface and they liberate CF_y to the gas phase (in addition to the ion components).

The oxide etch reactions are also found in Table 1. Reactions R7 are for etching on the monomer surface, which are assumed to produce CO along with a somewhat fluorine deficient SiF_2 product. The reactions are written such that monomer sites contribute one carbon and one fluorine and the reactions produce bare oxide surface. Reactions R8 depict the etching of fluorine-covered surface. This reaction can produce SiF_4, although it is written to produce SiF_2 and atomic fluorine. This is done assuming that SiF_4 will not survive in the plasma very long before being dissociated to smaller fragments. By using this simplification, only the major gas phase products are followed, which is important in the simulations to be discussed later. Along with SiF_2 and F, O_2 is assumed to be a product since these reactions are taking place on a carbon-deficient surface. Finally, reactions R9 depict (chemical) sputtering of the oxide surface with chemically reactive ions. The products, generally SiF and O_2, from these reactions are both fluorine and carbon deficient. The final reaction taken into account on the surface is that of chemical etching (not shown). Chemical etching is assumed to occur only on the fluorine-covered oxide surface.

2.3. Rate expressions

For adsorption reactions, a simple sticking coefficient rate expression was used. For ion-enhanced etching and sputtering reactions, a simple square-root dependence of sputtering yield on ion-bombardment energy was used [4–6,14,37].

$$Y = A\left(\sqrt{E_i} - \sqrt{E_{th}}\right) \tag{1}$$

In Eq. (1), Y is the yield, A is the so-called slope, E_i is the ion energy and E_{th} is the threshold energy. The chemical etch rate, was given by Flamm et al. [38,39].

The mathematical formulation of the proposed surface chemistry model is derived from a surface site balance [49], in which the total number of sites on the oxide surface is assumed to be constant. Site density values are then expressed as fractions of the total number of sites. Reactions occurring on a given type of coverage then have their rates multiplied by the corresponding site density fraction.

3. Parameter estimation

In producing a unified model such as the one presented here, it becomes imperative that as much information as possible is taken into account to obtain the various parameters used in the model. Trying to obtain values for the individual parameters in the model is a daunting task, and undoubtedly many have to be estimated or fit.

3.1. Sticking coefficients of neutral radicals

For the oxide surface, the sticking coefficient for fluorine atoms (reaction R1 in Table 1) is taken from the paper by Gray et al. [37]. They found a relatively constant sticking coefficient for F atoms on clean, damaged oxide surfaces to be 0.02. This value is comparable to the value measured by Tserepi et al. [23] on an aluminum substrate.

Fluorocarbon sticking coefficients are less straightforward because there are no direct measurements of the sticking coefficients of fluorocarbon radicals on clean oxide surfaces. This is due to the fact that impinging fluorocarbon radicals tend to form polymer films on exposed surfaces. In addition to the difficulty in ascertaining the state of the surface, there is added uncertainty because most measurements are actually of the surface reaction probability or the surface loss rate of CF_x's. The actual reaction pathway or any liberated product species after striking the surface is unknown. For instance, a CF radical may adsorb on a surface and stick, or it may recombine with a surface species such as adsorbed F and form gaseous CF_2 which would then still be measured as CF 'sticking' to the surface.

There have been several studies done to examine the surface loss coefficients of the fluorocarbon radicals on different surfaces. Hikosaka et al. [8,15], measured the surface loss coefficient of CF_2 and CF_3 on aluminum, stainless-steel, and polymer surfaces. Tserepi et al. [20,23], also measured the surface loss coefficient of CF_2 and CF_3 on aluminum and fluorocarbon surfaces, finding good agreement with Hikosaka et al. for the aluminum substrates. Thomas et al. [22] measured the surface loss coefficient of CF_2 on silicon surfaces. The value obtained corresponds well with the values found in the previous studies for aluminum and stainless steel. Finally, Booth et al. [19] measured surface loss rates for CF and CF_2 on aluminum. For CF_2, the surface loss coefficient was comparable to the previous studies, although slightly larger. The CF surface loss coefficient could not be measured accurately, but a lower limit of 0.14 was obtained.

Because of the uncertainty in the measurements and in the applicability of these measurements to the model system being developed, sticking coefficients for each radical on the oxide surface (reactions R2) are chosen to a single digit of precision. For CF, a value of 0.1 is used for the sticking coefficient on the clean oxide surface and a value of 0.2 is used on the activated polymer surface, similar to the sticking coefficient measured by Booth et al. For CF_2 and CF_3, a value of 0.005 is used on the clean oxide surface, while a value of 0.02 is used on the activated polymer surfaces. These values bracket the numbers reported in the literature for these radicals on metallic and fluorocarbon surfaces [8,15,19,20,22,23]. The sticking coefficients on the activated polymer surface should be of the same order as those on the clean oxide surface because both are produced only after exposure to sufficient ion bombardment and because the studies noted above show generally similar sticking coefficient behavior on different surface types exposed to ion bombardment.

Since neutral radical deposition on both monomer- and polymer-covered surfaces, (reactions R3), should be similar, the same sticking coefficients are assumed for both processes. From Bell et al. [1] and Rueger et al. [14], it may be seen that increases in gas pressure appears to affect the larger ion-energy regime more than the lower ion-energy regime. At low ion energies, the measured etch (and/or deposition) rates for different pressures appear to converge, which would require that activated polymer deposition dominates behavior under these conditions. If neutral deposition alone dominated, varying the pressure between 5 and 20 mtorr would result in differences in the deposition rate on the order of about four times, which is not seen. With this observation, a single non-ion-assisted

neutral deposition (reactions R3) sticking coefficient of 0.002 is assumed, since it should not affect the deposition behavior greatly, i.e. deposition is dominated by sticking of radicals on ion-activated sites. This value results in a neutral deposition rate of approximately 15 nm/min without ion bombardment. In the literature, values of deposition rate without external r.f. bias span from 50 to approximately 300 nm/min [1,4,5,11,14, 30,40]. However, measurement of deposition rate at zero ion bombardment is very difficult because the floating potential is always present, providing up to approximately 20 eV of energy without the presence of external biasing. In one experiment, a deposition enhancement factor due to ion bombardment, of between 2 and 6, was determined without external biasing [4]. If the neutral-only deposition rate from the model is multiplied by the upper end of this factor, the resulting deposition rate falls in the range of observed deposition rates without external biasing but with ion bombardment due to the floating potential.

3.2. Ion-driven reactions

With deposition rates in place, attention must now turn to the more complicated ion-driven reactions used in polymer activation and polymer and oxide etching. Before looking at specific reactions in the model, behavior associated with individual ions will be discussed.

In separate studies using ion beams of known composition, Mayer et al. [25,26], Miyake et al. [28], and Shibano et al. [29] saw enhanced reactivity of fluorocarbon ions containing larger amounts of fluorine (such as CF_2^+ and CF_3^+). In Mayer et al. [25], the etch yields of SiO_2 were investigated and the relative yields of the different fluorocarbon ions followed the degree of fluorination of the ions. The ion reactivities were 6.1, 3.2, 1.8 and 0.4, respectively, for CF_3^+, CF_2^+, CF^+, and F^+, at 500 eV bombardment energy. Also shown in their paper were results for silicon etching with the various fluorocarbon ions, which also showed a progression of reactivity based on the amount of fluorine in the impinging ion. In Miyake et al. [28], mass-selected fluorocarbon ion bombardment of Si was examined. The results showed a peak of reactivity for fluorocarbon ions at lower ion-bombardment energies. In this region (< 1 keV), yields of the fluorocarbon ions generally followed the progression $CF_3^+ > CF_2^+ > F^+ > CF^+$. Approximate yields at 500 eV bombardment energy were 0.33, 0.25, 0.18 and 0.07 for the order shown.

In addition to these studies, Shibano et al. [29] examined SiO_2 etching with mass-selected CF_x^+ beams. Etch yields increased following the order $CF_3^+ > CF_2^+ > CF^+ \sim F^+$. At ion energies above approximately 200 eV, CF_3^+ and CF_2^+ separated into the order shown above, while the behavior of CF^+ and F^+ remained obscured over much of the ion bombardment energy range due to fluorocarbon deposition. In the case of CF^+, the deposition was particularly pronounced, leading to the conclusion that CF^+ is more reactive compared to the other fluorocarbon ions in activating the surface for polymer deposition.

In all the studies mentioned above, there was an uncontrolled neutral flux to the surfaces being studied. Thus, there is a good chance that neutral deposition and ion-enhanced neutral reactions are affecting results reported in their systems.

3.3. Polymer activation and sputtering

Looking at polymer activation first, there are two factors that help determine the parameters for reactions R5. The first is the eventual deposition rate expected with both neutral-only and ion-enhanced deposition. As mentioned in the discussion of sticking coefficients in the model (Section 3.1), deposition rates between 50 and 300 nm/min have been observed in experimental systems [1,4,5,11,14,30,40]. Therefore, the activated deposition rate produced by the model should fall in this range of values. In addition, an upper limit on the amount of activated deposition is evident by again using the behavior of the system with changing pressure. If too much activated coverage is produced, activated polymer growth will increase by a large amount with an increase in pressure, which is not observed experimentally [4,5,14]. Along with these trends, work done by Shibano et al. [29] showed increased ability of CF^+ to activate the surface.

There is little to no information on ion-assisted etching of fluorocarbon polymers in general, although there is some data in studies by Oehrlein et al. [4,14]. Unfortunately, data taken in these studies is for different chemistries and plasma sources and the neutral fluxes of the various fluorocarbon species are unknown. Both threshold energy and slope values for the polymer etch reactions [Eq. (1)] are assumed to follow the progression of reactivities found in the studies by Mayer et al. [25,26], Shibano et al. [29] and Miyake et al. [28]. The threshold values affect the ion energy at which the maximum deposition rate occurs. In Oerhlein et al. [4,14], these maxima are found at energies of approximately 30–60 eV or below. Therefore, a threshold value of 60 eV is used for CF^+ etching of polymer and progressively lower values are used for CF_2^+ and CF_3^+. The slope values are fit to generate a deposition to etching cross-over point between 30 and 60 eV, as observed experimentally by Oehrlein et al.

3.4. Oxide etching

The next set of parameters to be examined govern the oxide etching regime at high (> 200 eV) ion-bombardment energy. There are three kinds of ion-

driven etch reactions, listed in Table 1 as R7–R9: etching of the monomer-covered surface; etching of the fluorine-covered surface; and chemical sputtering of the bare oxide to produce products with less fluorine and carbon. The same yield parameters are used for etching the monomer-covered and fluorinated surfaces. The fluorinated surface is assumed to produce more fluorinated products with little CO. The monomer coverage is assumed to produce a less fluorinated product, and forms CO more readily. In either case, reactions R7 and R8 are assumed to represent the mechanism that produces the results seen in the literature, since in all the cases involving etching with fluorocarbon plasmas or beams, there is evidence of surface modification due to adsorption of either neutrals or ionic fragments [4,24–27,29].

In the case of chemical sputtering, fluorocarbon ions with sufficient energy impinging on the bare oxide surface may produce etching of the oxide, although the site density of the bare oxide remains unchanged, see reactions R9 in Table 1. There is little information on direct reactive sputtering reactions because of the difficulty involved in studying these reactions while keeping the surfaces clean. However, there are pure sputtering reactions reported in studies using argon ions to bombard what may be assumed to be clean SiO_2 surfaces. These sputtering reactions show an approximate order of magnitude drop in yield at a given ion energy. The reactivity of fluorocarbon ions impinging on bare SiO_2 surfaces should probably be between the reactivity of ion-assisted etch reactions (in the presence of fluorocarbon radicals) and the Ar^+ sputtering yields on clean surfaces.

The final set of parameters should mirror both the increase in yield when etching a monomer or fluorine covered surface compared to a bare oxide surface and the differences in reactivity observed between the various fluorocarbon ions. The final parameters chosen for the yield expressions governing these reactions produce yields in the range of observed yield data found in the literature involving fluorocarbon etching of SiO_2 [1,5,14,24,25,27,29,42]. Since information on chemical sputtering, reactions R9, is scarce, the parameters for etching on the bare oxide have been estimated to produce yields about an order of magnitude lower than the comparable reactions on monomer or fluorine covered surfaces.

The differences in the yields of the various fluorocarbon ions used in the present model mirror the differences in yield observed in beam studies [25,26,28,29]. Both the slope and the threshold energy values have been selected to reflect these differences. The more fluorinated ions are assumed to be three to five times more reactive than the lesser-fluorinated CF^+ ion and the lighter and carbon-deficient F^+ ion.

3.5. Chemical etching

As a final note, the last reaction taken into account in the model is that of chemical etching. Chemical etching makes almost no contribution (on the order of 10 nm/min or less) to the final measured oxide etch rate since SiO_2 etches so slowly in an atomic fluorine environment without ion bombardment [38,39,43]. The corresponding reaction parameters are taken directly from Flamm et al. [38,39] and correspond to spontaneous etching of fully fluorinated SiO_2 in a fluorine atmosphere.

3.6. Sensitivity analysis

The large number of parameters in the model necessitates at least a rudimentary sensitivity analysis of the effect of these parameters on the computed results. Oxide etching with fluorocarbon plasmas is an extremely difficult problem from the gas phase and especially the surface chemistry point of view. However, the surface chemical effects can at least be separated according to the ion energy regime. For instance, the oxide etching yields are irrelevant at low energies where polymer deposition actually occurs. Similarly, the polymer sputtering yields are not important at high ion energies where there is hardly any polymer on the oxide surface. By focusing on the three separate regimes of oxide etching behavior (polymer deposition, polymer suppression or transition to etching and oxide etching, see Fig. 1), the most important parameters within each of these regimes may be identified.

Sensitivity analysis of the surface chemistry model was performed by varying the parameter value by a factor of two in either direction. The most important parameters governing oxide etch rate were the sticking coefficient for CF on bare oxide, and the yield of the CF_3^+ reaction on both fluorinated and monomer-covered oxide (reactions R2 in Table 1). The polymer deposition rate at very low ion energies was affected by the sticking coefficient on the polymer surface. At higher ion energies (but still within the polymer deposition regime), the slope of the CF^+ polymer activation reaction, and the threshold energy for polymer etching by CF_3^+ ion impact were most important. Finally, the major parameter controlling the transition point between deposition and etching was also the threshold energy for polymer etching by CF_3^+. The transition energy almost doubles when the threshold is doubled and more than halves when the threshold is halved.

4. Plasma simulation

In order to investigate the behavior of the surface chemistry model under reactive ion etching conditions, the model was implemented, along with a plasma chemistry set, within a plasma simulation tool known as

MPRES, or Modular Plasma Reactor Simulator [44–46]. MPRES is a finite element-based fluid model designed to determine the steady-state solution of the various species densities and the electron-energy associated with a given plasma chemistry and reactor geometry for an inductively-coupled plasma (ICP) reactor. The simulator assumes cylindrical symmetry, thereby reducing the problem to two dimensions, r and z. The reactor geometry and chemistry (both gas and surface chemistry) are incorporated through user-provided input files. The simulation generates an output file consisting of contour data for the species densities, electron temperature, power deposition and plasma potential throughout the plasma region. Surface coverages along the reactor boundaries are also produced.

MPRES uses an equation splitting algorithm to enhance the speed at which the simulation converges to the steady-state solution. The simulation solves the equations associated with each of the unknown types (neutral densities, ion and electron densities and electron energy), on their own natural time scales. Stiffness in space is dealt with by splitting the plasma into bulk and sheath regions and solving each separately. The characteristic length scale of the reactor, which would be on the order of meters, is four orders of magnitude greater than the length scale of the sheath. This introduces problems in producing a grid capable of capturing the sheath while still spanning the rest of the plasma. Splitting the simulation into bulk plasma and sheath modules overcomes this problem.

The gas-phase reaction set was taken from Johannes et al. [54]. A more complete set with additional species and reactions was tested in a 0-D model in which transport phenomena are ignored and the reactor volume is assumed to hold a single average density for each of the species under investigation. The advantage of this type of analysis is that instead of following the densities of a limited number of species throughout the plasma region, the 0-D model may follow a much larger number of species and a much greater number of reactions or surface interactions. The 'important' species and reactions may then be used in the 2-D simulator (MPRES), which has much greater computer resource requirements than the simpler 0-D model but also gives much more detailed information about the spatial profiles in the reactor. The following gas-phase species were included in the simulation: C_2F_6; CF_4; CF_3; CF_2; CF; F; SiF_2; SiF; O_2; CO; CF_3^+; CF_2^+; CF^+; F^+; and CF_3^-.

5. Results and discussion

5.1. Validation

Oxide etching was studied in the reactor shown schematically in Fig. 3. It is a standard inductively

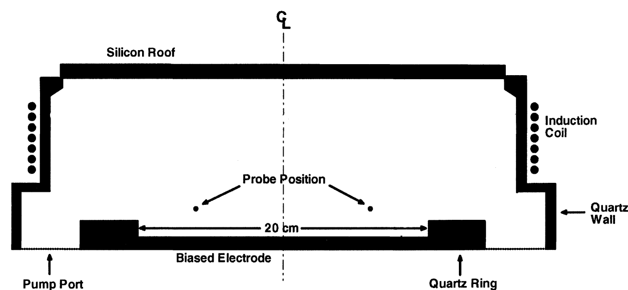

Fig. 3. Schematic of the reactor employed in this study. Seven turns of an inductive coil are wrapped around the quartz sidewall. Calculations of ion flux, neutral density, and average F/C ratio of ion flux for Figs. 7–9 were done at the 'probe position' location.

coupled plasma reactor with a solenoidal coil wrapped around the cylindrical quartz sidewall. The oxide covered wafer rests on the bottom electrode, which can be biased independently by a separate r.f. power supply. A quartz ring holder surrounds the etching surface as shown in Fig. 3. The silicon roof is maintained at relatively high temperatures (245–275°C) to consume F atoms and 'load' the reactor. This effectively controls the C/F ratio in the gas phase and hence the degree of polymer deposition in the system. The quartz walls are also hot (200°C) to minimize polymer deposition on the walls. Base case conditions are as follows: source power 2600 W, bias power 1250 W, pressure 5 mtorr and flow rate of pure C_2F_6 30 sccm. Using the given bias power (P_{bias}) and the calculated ion flux (I_i), an ion energy (E_i) was estimated from

$$P_{bias} = I_i \times E_i \tag{2}$$

In oxide etching by fluorocarbon plasmas, it is believed that there exists a thin fluorocarbon polymer layer on the surface at steady state. Ions bombarding the surface can dissipate part of their energy during transit through this polymer layer before reaching the oxide surface. At the high bias voltages (and ion energies) used in this study (above 350 eV), the polymer layer is expected to be very thin (a monolayer or less), and all ion energy is used for etching/chemical sputtering reactions.

There are three major surface types (boundaries) found in the reactor: the oxide covered wafer (biased electrode) surface; the silicon roof; and the quartz walls. Although interest in this study centers around the behavior of the oxide-covered wafer, the other surfaces in the reactor must be taken into account as well. Surface reactions taken into account on the heated silicon roof and on the quartz walls and ring are shown in Table 2. The silicon roof is etched by impinging fluorine radicals with a surface loss probability given by [28,39,47]. The reaction generates SiF_4 as the major product, which is assumed to quickly dissociate in the gas phase resulting in SiF_2 and 2F. Other reactions

Table 2
Surface reactions on silicon roof and quartz walls

Reaction		Surface loss probability
Quartz walls		
CF_3^+	$\rightarrow CF_3$	0.6
	$\rightarrow CF_2 + F$	0.4
$2CF_3$	$\rightarrow C_2F_6$	0.01
CF_2^+	$\rightarrow CF_2$	0.70
	$\rightarrow CF + F$	0.28
	$\rightarrow SiF_2 + CO_2$	0.02 (etching)
CF^+	$\rightarrow CF$	1.0
F^+	$\rightarrow F$	1.0
Silicon roof		
CF_3^+	$\rightarrow CF_3$	0.7
$2CF_3^+$	$\rightarrow 2CF_2 + SiF_2$	0.3 (etching)
$2CF_3$	$\rightarrow C_2F_6$	0.01
CF_2^+	$\rightarrow CF_2$	0.8
$2CF_2^+$	$\rightarrow 2CF + SiF_2$	0.2 (etching)
CF^+	$\rightarrow CF$	1.0
F^+	$\rightarrow F$	1.0
4F	$\rightarrow SiF_2 + 2F$	0.04 (etching)

include surface impact dissociation, in which a more fluorinated CF_x^+ ion hits a surface and breaks into CF and fluorine radicals. These reactions are assumed based on the work of Mitsuoka et al. [3], in which low-energy ions were irradiated on metallic surfaces and significant fragmentation of the parent ion was detected. The walls are not significant sinks for CF_x radicals since high wall temperatures have been shown to suppress fluorocarbon deposition [9].

The surface chemistry model (Fig. 1) reproduces all trends seen in oxide etching, namely ion-assisted deposition at low ion energies, transition to oxide etching at intermediate ion energies and roll over of the oxide etch rate at high ion energies [4,14].

In Fig. 4, the predicted etch rate profiles (lines) are compared with experimental data (lines with points) for the base case conditions [48]. The predicted oxide etch rate increases monotonically from the wafer center to the edge. The simulated etch rate is in qualitative agreement with the experimental data. As bias power is increased (from curve a to curve b) for a constant inductive power, the etch rate also increases. The increase in etch rate with bias power, however, is only slight. This can be explained as follows: under a constant inductive power, the total ion flux to the surface remains essentially constant. Therefore, an increase in bias power results in a corresponding increase of the ion energy [Eq. (2)]. Now, the dependence of all ion-assisted reactions on ion energy was assumed to be given by Eq. (1), i.e. a square root dependence. However, the etch rate increases less than what would be predicted by the square root dependence, due to the fact that the surface coverage of reactants (monomer and fluorine coverage, see Fig. 2) is reduced as the ion energy increases (surface adsorbates are used up in etching reactions).

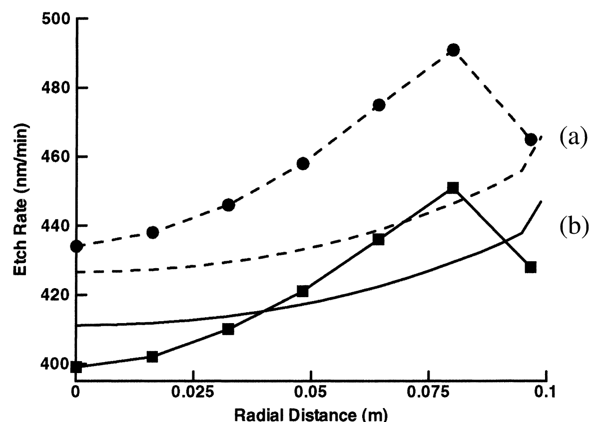

Fig. 4. Predicted oxide etch rate profiles compared with experimental data [48]. (a) 1250 W bias power: (solid line, simulation; solid line with squares, experiment). (b) 1550 W bias power: (dotted line, simulation; dotted line with circles, experiment). Drop of experimental etch rate at the edge may be due to the wafer clamp.

5.2. Simulation runs

In the following discussion, each figure with contour plots contains results for two species, one on each side, with the axis of symmetry at $R = 0.0$ m. Radial profiles of fluxes and etch rates (uniformity) are presented

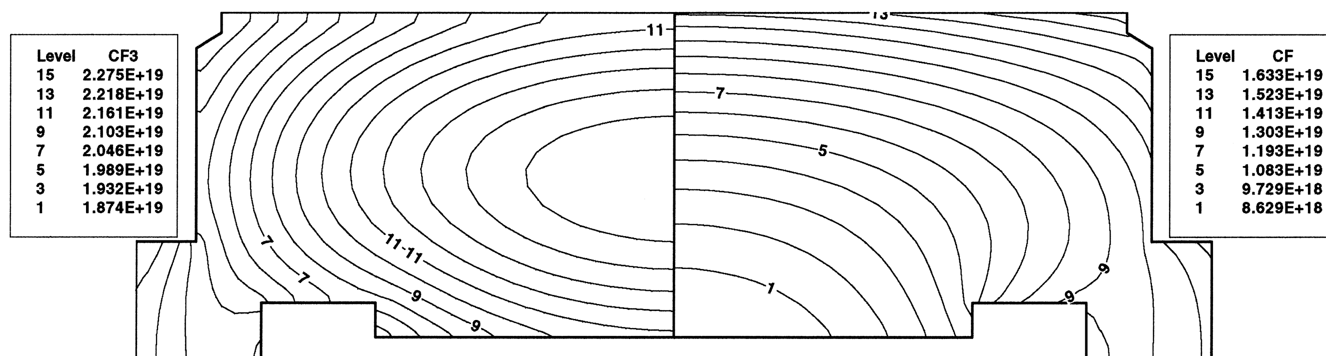

Fig. 5. CF_3 (left) and CF (right) fluorocarbon radical densities for the base case conditions.

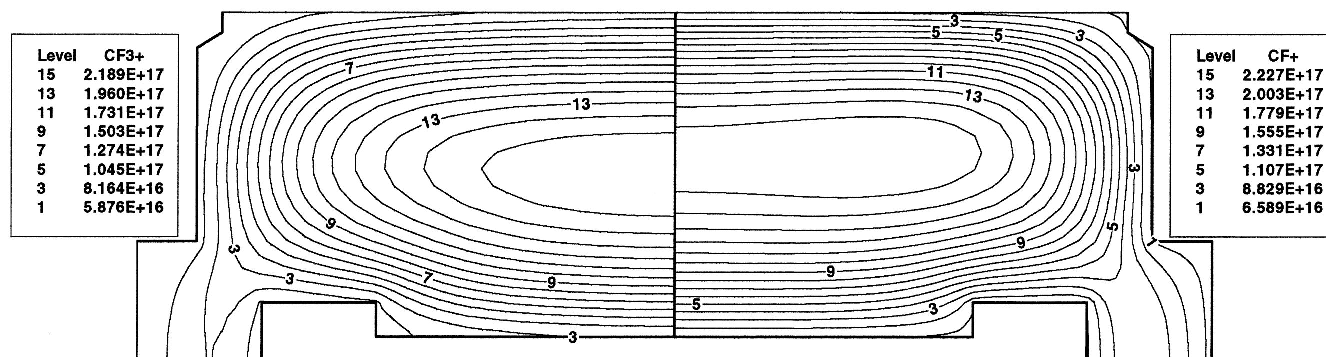

Fig. 6. CF_3^+ (left) and CF^+ (right) ion densities for the base case conditions.

separately. For these graphs, 'edge-fast' implies a higher value at the edge of the wafer, while 'center-fast' refers to a peak in the center of the wafer.

MPRES simulation results showed that, under the base case conditions (5 mtorr, 2600 W inductive power, 1250 W bias power corresponding to 370 eV ion energy, and 30 sccm of C_2F_6), the dominant neutral species in C_2F_6 plasma is CF_3. This has been verified experimentally under comparable conditions [50,51]. Density profiles of CF_3 and CF radicals are plotted in Fig. 5. The CF_3 density peaks in the center of the reactor, while the CF density shows a maximum at the corner between the silicon roof and the quartz sidewall (upper right corner) and a minimum on the oxide surface. The density profile of CF_2 (not shown) was similar to that of CF. CF_3 radicals are dissociated near the coils and are reacting on the wafer surface. Hence, their density peaks at the reactor center. On the other hand, CF is produced near the coils by gas phase dissociation of CF_x ($x = 2, 3$) and also by ions neutralizing and at the same time dissociating upon impact on the walls [53]. Because the walls are maintained at relatively high temperatures, deposition of fluorocarbon film is negligible and radicals generated by ion impact return to the gas phase [52]. Surface reactions appear to be the main cause of the concentration gradient of CF radicals, when compared to CF_3.

Fig. 6 shows density profiles of the major fluorocarbon ions, CF_3^+ and CF^+. The peak densities of these ions are comparable under the base case conditions. The two ions show slightly different radial profiles, however. Compared to CF_3^+, the CF^+ density is more elongated in the radial direction and the maximum density is locates closer to the quartz sidewall. This can be understood from the fact that the CF neutral radical density profile peaks nearer the sidewalls. On the other hand, the CF_3 radical density peaks at the reactor center. The negative ion density (not shown) was two to three times greater than the electron density.

Li et al. [50], reported ion fluxes and fluorocarbon neutral densities in inductively coupled C_2F_6 plasmas near the oxide surface (at the 'probe position' location, see Fig. 3). Several trends in their measurements are similar to those produced by the simulation as shown in Fig. 7. The total ion flux increases roughly linearly with power. The CF^+ and CF_2^+ ion fluxes also increase with inductive power whereas the CF_3^+ ion flux remains nearly constant. The most abundant ionic species is predicted to be CF_3^+ at low inductive power and CF^+ at high inductive power. Li et al, however, measured CF_3^+ to be the most abundant ion throughout the power range of their investigation. It is conceivable that the actual power dissipated in the their plasma is considerably smaller than the measured power. Other differences between the experimental and simulated systems can relate to the wall conditions. In the simulated reactor, the walls are hot to prevent polymer deposition. In contrast, polymer may deposit on the walls of the experimental reactor used by Li et al. Due to the coupling between gas phase and surface chemistries, this difference can account for differences in the observed behavior.

Fig. 8 depicts the variation of neutral densities when the inductive power is changed. CF_3 is the most abundant neutral radical within the range of inductive power shown. As the inductive power increases from 800 to 4000 W, the CF_3 radical density decreases and the CF

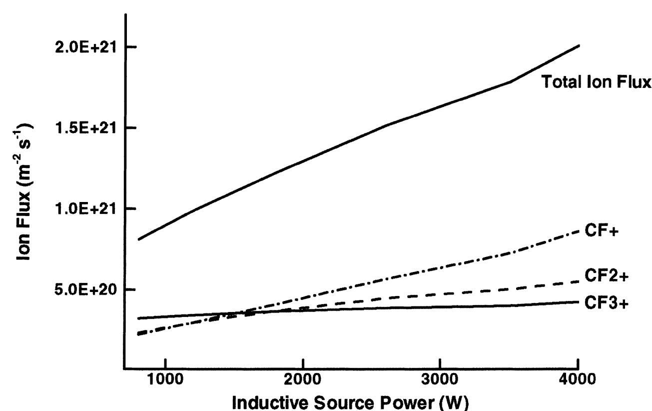

Fig. 7. Flux of fluorocarbon positive ions at the probe position in Fig. 3 as a function of inductive power. Other conditions at the base case values. The total ion flux also included F^+.

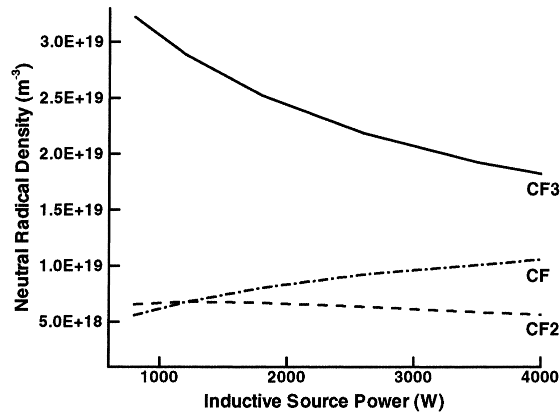

Fig. 8. Densities of fluorocarbon neutral radicals at the probe position in Fig. 1 as a function of inductive power. Other conditions at the base case values.

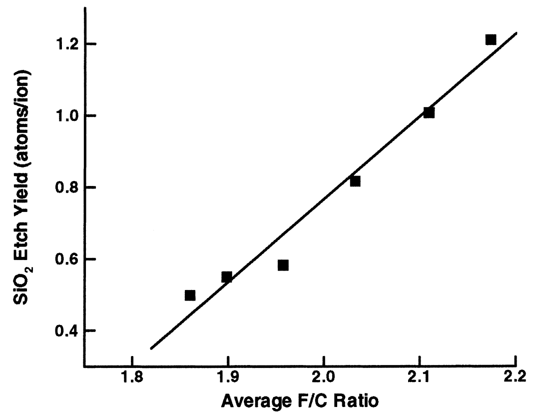

Fig. 9. Oxide etch yield as a function of the average F/C ratio of ion flux at the probe position. The inductive power was varied from 800 to 4000 W. Other conditions at the base case values. The etch yield is defined as number of atoms etched per incident ion.

radical density increases. In contrast, the CF_2 density increases only slightly and then decreases. This behavior is typical of consecutive reactions of the type $CF_3 \rightarrow CF_2 \rightarrow CF$, whereby further dissociation to the less fluorinated radicals occurs as the electron density in the plasma (inductive power) is increased.

The oxide etch rate as a function of inductive power was found to increase monotonically assuming that the bias voltage (hence bias power) was adjusted to maintain the same ion bombardment energy. When the bias voltage was fixed, however, the relation between etch rate and inductive power is not that simple. In fact, the etch rate can decrease with increasing power. This is due to the fact that, as inductive power is increased, the ion flux to the surface also increases. For a constant bias power this corresponds to lowering the ion bombardment energy [see Eq. (2)].

It was further found that the oxide etching yield is linearly proportional to the F/C ratio in the incident ion flux as shown in Fig. 9. This has also been found experimentally [50]. It is noted in passing that the total ion flux increases with inductive power (Fig. 7) but the F/C ratio of the incident ion flux decreases. Since the etch rate is the product of the ion flux with the etch yield, it is expected that the etch rate will increase slower with inductive power (smaller slope of the etch rate vs. power curve) as power increases. This is indeed what is observed in the simulation.

Plasma species and etch rate profiles can also be affected by gas pressure. The profiles of CF_3^+ ion density at 10 and 20 mtorr pressure are plotted in Fig. 10. Reference should also be made to Fig. 6 (left) where the corresponding profile at 5 mtorr is shown. The peak density of CF_3^+ increases as the pressure is increased from 5 to 20 mtorr. At 10 mtorr, the CF_3^+ density peak is more elongated towards the sidewall. At 20 mtorr the ion density peaks off axis near the power deposition zone. As pressure is increased, ion diffusivity and mobility are both reduced. Hence, the ion density is higher nearer the production zone, i.e. near the coils.

The total flux of F- and C-containing neutral radicals to the oxide surface peaks at the edge of the wafer (Fig. 11a). In contrast, the total flux of F- and C-containing ions peaks at the wafer center (Fig. 11b). Now, oxide etching is ion driven; etching does not occur without ion bombardment (in fact polymerization will occur in that case). Hence, one might expect that the oxide etch

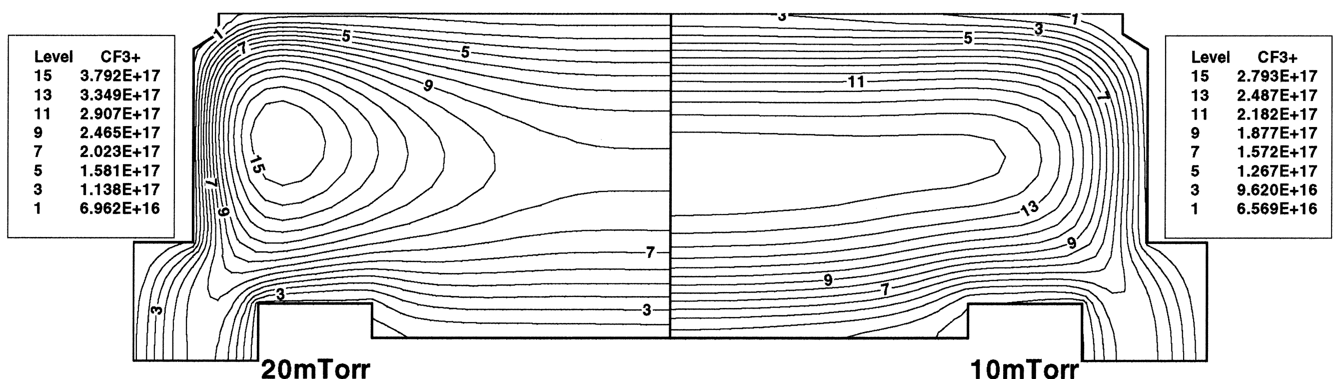

Fig. 10. CF_3^+ ion density contours at 20 (left) and 10 mtorr (right). Other conditions at the base case values.

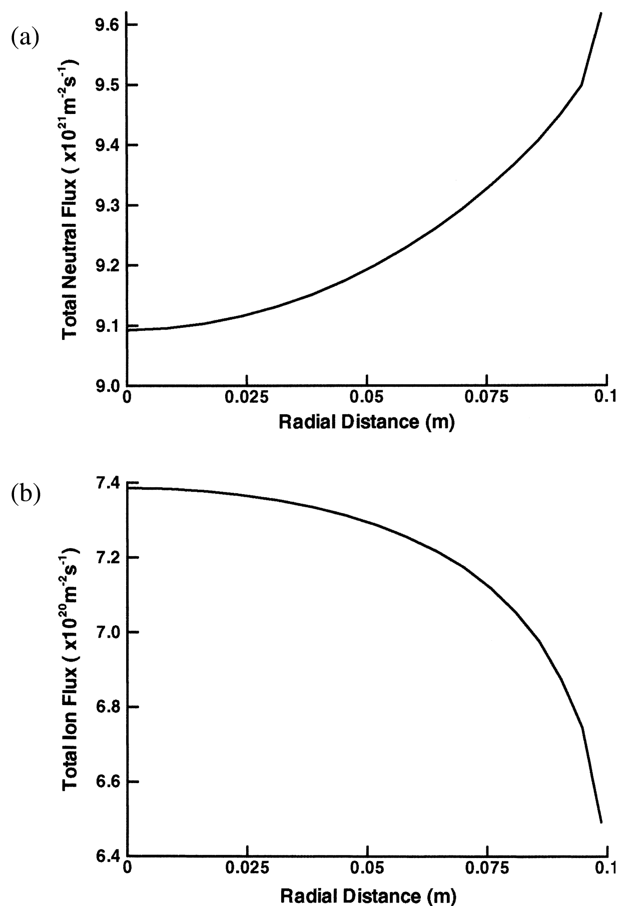

Fig. 11. Total (CF_x plus F) neutral flux (a), and total (CF_x^+ plus F^+) ion flux (b), on the wafer surface vs. radius. Conditions were at the base case values.

rate profile would follow the shape of the ion flux profile (center fast). Instead, the etch rate follows the shape of the neutral flux profile (edge fast, see Fig. 4). This is because at the low pressure of 5 mtorr, the system is neutral starved. The surface coverage of reactive species (not shown) increases from the center to the edge of the wafer and this drives the reaction faster at the edge. Further evidence is provided by looking at the radial profiles of total ion flux and etch rate as a function of gas pressure (Figs. 12 and 13). At 5 mtorr, etching is neutral starved and the etch rate follows the neutral flux profile (edge fast), which is opposite from the ion flux profile (center fast). At 20 mtorr, etching is ion starved (the neutral density is now up roughly by a factor of 4 compared to 5 mtorr), the etch rate follows the ion flux profile. At the intermediate pressure of 10 mtorr, the profile is in-between the neutral and ion flux profiles and is most uniform. This also suggests an optimum pressure where etch uniformity is best.

It is interesting to note that the total ion flux to the wafer decreases with increasing pressure (Fig. 12), despite the fact that the total ion density in the bulk of the reactor increases with pressure (not shown). This is due to stronger density gradients as pressure increases and also lower electron temperature, which lowers the Bohm flux of ions to the surface. On the other hand, the oxide etch rate is seen to increase with pressure (Fig. 13), a result of increased surface coverage of reactants. These results again underscore the interplay of ion bombardment flux/energy and surface coverage in deciding the oxide etch rate and uniformity.

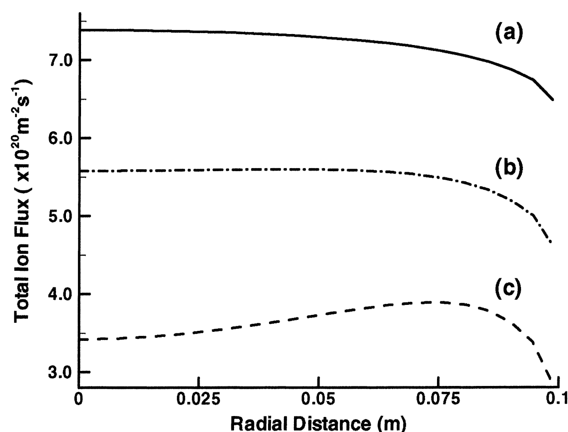

Fig. 12. Total (CF_x^+ plus F^+) ion flux (a), and oxide etch rate (b), vs. wafer radius for three different reactor pressures; (a), (b), and (c) correspond to 5, 10, and 20 mtorr, respectively. Other conditions were at the base case values.

6. Conclusions

Fluorocarbon plasmas have been studied extensively because of their use in selectively etching oxide over silicon. It is widely known that these plasmas produce unsaturated fluorocarbon radicals that may polymerize on surfaces in contact with the plasma. Oxide surfaces exposed to intense ion bombardment, on the other hand, are etching.

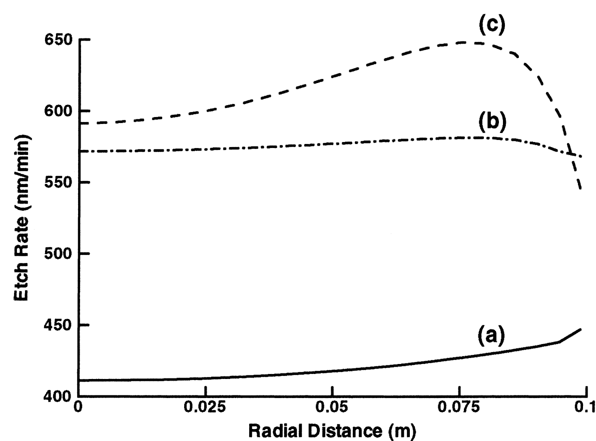

Fig. 13. Oxide etch rate vs. wafer radius for three different reactor pressures; (a), (b), and (c) correspond to 5, 10, and 20 mtorr, respectively. Other conditions were at the base case values.

In this work, a comprehensive coupled plasma/surface chemistry model was developed to understand the mechanism of etching or deposition on oxide surfaces exposed to a high density C_2F_6 plasma. The chemistry models were implemented in the Modular Plasma Reactor Simulator (MPRES) code, to study oxide etching and uniformity under typical processing conditions.

Simulation results duplicated several trends observed experimentally: ion-assisted deposition at low ion energies, transition to polymer suppression and oxide etching at higher ion energies, increases in etch rate with increasing pressure, and a slight decrease in etch rate with increasing source power (at constant bias power). In addition, the experimentally observed etch profile across the radius of the wafer was captured. For the conditions examined, CF_3^+ and CF_3 were predicted to be the most important ion and radical, respectively, in the system as observed experimentally under comparable conditions.

Along with duplicating the experimentally observed behavior, several conclusions about the causes of this behavior were drawn. Under many of the conditions investigated, a competition between two opposing forces was evident. Understanding the two opposing forces produces a better understanding of the problem as a whole. Investigating the behavior of the system with changing bias power and inductive power sheds light on the competition that exists between ion fluxes and energies and neutral surface coverages. Increases in bias power lead to increases in the calculated raw etch yield, but may also deplete reactants from the surface to be etched. Increases in inductive power lead to increases in the ion flux and decreases in ion energy (for constant bias power). The first increases etch rates while the second depresses them. The model explains the etch-rate enhancement with increasing pressure by monitoring the surface coverages involved in oxide etching. The system is neutral starved at low pressures (5 mtorr). Therefore, increases in pressure lead to increases in the reactive coverages on the surface, which in turn drive etch rates higher.

Along with explaining changes in etch rate with changing conditions, the simulations also give an explanation of the etch profiles seen across the wafer at low pressures (5 mtorr). In the model, the ions have been assumed to be the only species with enough energy to induce etching or sputtering, and the profile of the ion flux across the wafer was 'center-fast'. The profile of the etch rate, on the other hand, was 'edge-fast', which corresponds well to both the fluorocarbon flux and reactive surface coverage profiles across the wafer. The surprising aspect of this result is that, although ions are the only species that drive surface chemistry, neutrals adsorbed on the surface control the etch profile across the wafer. This supports the conclusion that, under these conditions, etching is ion driven but neutral dominated.

Acknowledgements

This work was supported by Sandia National Laboratories/SEMATECH and the National Science Foundation. Many thanks to J. Johannes of Sandia National Labs and E. Meeks of Reaction Design for their help with fluorocarbon chemistry model development. We are also grateful to Dr T. Dalton for sharing experimental data taken while at Digital Equipment Corporation.

References

[1] F.H. Bell, O. Joubert, G.S. Oehrlein, Y. Zhang, D. Vender, J. Vac. Sci. Technol. A 12 (2) (1994) 3095–3101.
[2] K. Kubota, H. Matsumoto, H. Shindo, S. Shingubara, Y. Horike, Jpn. J. Appl. Phys. Part 1 34 (4B) (1995) 2119–2124.
[3] Y. Mitsuoka, H. Toyoda, H. Sugai, Jpn. J. Appl. Phys. Part 2 34 (11A) (1995) L1486–L1489.
[4] G.S. Oehrlein, Y. Zhang, D. Vender, M. Haverlag, J. Vac. Sci. Technol. A 12 (2) (1994) 323–332.
[5] G.S. Oehrlein, Y. Zhang, D. Vender, O. Joubert, J. Vac. Sci. Technol. A 12 (2) (1994) 333–344.
[6] C.h. Steinbruchel, H.W. Lehmann, K. Frick, J. Electrochem. Soc. 132 (1) (1985) 180–185.
[7] M. Haverlag, E. Stoffels, W.W. Stoffels, G.M.W. Kroesen, F.J. de Hoog, J. Vac. Sci. Technol. A 12 (6) (1994) 3102–3108.
[8] Y. Hikosaka, H. Toyoda, H. Sugai, Jpn. J. Appl. Phys. Part 2 32 (3A) (1993) L353–L356.
[9] S. Ito, K. Nakamura, H. Sugai, Jpn. J. Appl. Phys. Part 2 33 (9A) (1994) L1261–L1264.
[10] G. Ito, K. Nakamura, H. Sugai, Jpn. J. Appl. Phys. 62 (2) (1987) 662–672.
[11] Y. Gotoh, T. Kure, Jpn. J. Appl. Phys. Part 1 34 (4B) (1995) 2132–2136.
[12] K. Takahashi, M. Hori, T. Goto, Jpn. J. Appl. Phys. Part 1 33 (8) (1994) 4745–4751.
[13] T. Fukasawa, A. Nakamura, H. Shindo, Y. Horiike, Jpn. J. Appl. Phys. Part 1 33 (4B) (1994) 2139–2144.
[14] N.R. Rueger, J.J. Beulens, M. Schaepkens, M.F. Doemling, J.M. Mirza, T.E.F.M. Standaert, G.S. Oehrlein, J. Vac. Sci. Technol. A 15 (4) (1997) 1881–1889.
[15] Y. Hikosaka, H. Sugai, Jpn. J. Appl. Phys. Part 1 32 (6B) (1993) 3040–3044.
[16] M. Haverlag, W.W. Stoffels, E. Stoffels, G.M.W. Kroesen, F.J. de Hoog, J. Vac. Sci. Technol. A 14 (2) (1996) 384–390.
[17] K. Miyata, M. Hori, T. Goto, J. Vac. Sci. Technol. A 15 (3) (1997) 568–572.
[18] T. Arai, M. Goto, D. Takayama, T. Shimizu, M. Murakami, K. Horikoshi, H. Fujioka, Jpn. J. Appl. Phys. Part 2 34 (10B) (1995) L1392–L1394.
[19] J.P. Booth, G. Hancock, N.D. Perry, M.J. Toogood, J. Appl. Phys. 66 (11) (1989) 5251–5257.
[20] A.D. Tserepi, J. Derouard, J.P. Booth, N. Sadeghi, J. Appl. Phys. 81 (5) (1997) 2124–2130.
[21] K. Sasaki, Y. Kawai, C. Suzuki, K. Kadota, J. Appl. Phys. 82 (12) (1997) 5938–5943.
[22] J.W. Thomas, J.R. Suzuki, S.H. Kable, J.I. Steinfeld, J. Appl. Phys. 60 (8) (1986) 2775–2777.
[23] A. Tserepi, W. Schwarzenbach, J. Derouard, N. Sadeghi, J. Vac. Sci. Technol. A 15 (6) (1997) 3120–3126.

[24] J.M.E. Harper, J.J. Cuomo, P.A. Leary, G.M. Summa, H.R. Kaufmanm, F.J. Bresnock, J. Elecrochem. Soc. 128 (5) (1981) 1077–1083.

[25] T.M. Mayer, R.A. Barker, J. Elecrochem. Soc. 129 (3) (1982) 585–591.

[26] T.M. Mayer, R.A. Barker, J. Vac. Sci. Technol. 21 (3) (1982) 757–763.

[27] T.M. Mayer, R.A. Barker, L.J. Whitman, J. Vac. Sci. Technol. 18 (2) (1981) 349–352.

[28] K. Miyake, S. Tachi, K. Yagi, T. Tokuyama, J. Appl. Phys. 53 (4) (1982) 3214–3219.

[29] T. Shibano, N. Fujiwara, M. Hirayama, H. Nagata, K. Demizu, Jpn. J. Appl. Phys. 29 (10) (1993) 2336–2338.

[30] F. Fracassi, E. Occhiello, J.W. Coburn, J. Appl. Phys. 62 (9) (1987) 3980–3981.

[31] N. Ikegami, N. Ozawa, Y. Miyakawa, M. Konishi, J. Kanamori, Jpn. J. Appl. Phys. 29 (10) (1990) 2236–2242.

[32] J.P. Simko, G.S. Oehrlein, J. Electrochem. Soc. 138 (9) (1991) 2748–2752.

[33] J. Ding, J.-S. Jenq, G.-H. Kim, H.L. Maynard, J.S. Chamers, N. Hershkowitz, J.W. Taylor, J. Vac. Sci. Technol. A 11 (4) (1993) 1283–1288.

[34] J. Ding, N. Hershkowitz, Appl. Phys. Lett. 68 (1996) 1619–1621.

[35] A. Misaka, K. Harafuji, M. Kubota, N. Nomura, Jpn. J. Appl. Phys. Part 1 31 (12B) (1992) 4363–4369.

[36] J.S. Han, J.P. McVittie, J. Zheng, J. Vac. Sci. Technol. B 13 (4) (1995) 1899–1983.

[37] D.C. Gray, I. Tepermeister, H.H. Sawin, J. Vac. Sci. Technol. B 11 (4) (1993) 1243–1257.

[38] D.L. Flamm, V.M. Donnelly, D.E. Ibboston, J. Vac. Sci. Technol. B 1 (1) (1983) 23–30.

[39] D.L. Flamm, V.M. Donnelly, J.A. Mucha, J. Appl. Phys. 52 (5) (1981) 3633–3639.

[40] K. Takahashi, M. Hori, M. Inayoshi, T. Goto, Jap. J. Appl. Phys. Part 1 35 (6A) (1996) 3635–3641.

[41] N. Ikegami, N. Ozawa, Y. Miyakawa, M. Konishi, J. Kanamori, Jpn. J. Appl. Phys. 30 (7) (1991) 1556–1561.

[42] A. Barbara, J. Heath, Electochem. Soc. 129 (2) (1982) 396–402.

[43] Y.-Y. Tu, T.J. Chuang, H.F. Winters, Phys. Rev. B 23 (2) (1981) 823–835.

[44] D.J. Economou, J. Feldsien, R.S. Wise, Transport and reaction in inductively coupled plasmas for microelectronics, Electron Kinetics and applications of Glow Discharges, NATO Advanced Research Workshop, Plenum, 1998.

[45] R.S. Wise, D. Lymberopoulos, D.J. Economou, Plasma Sources Sci. Technol. 4 (1995) 317–331.

[46] R.S. Wise, D. Lymberopoulos, D.J. Economou, Appl. Phys. Lett. 68 (1996) 2499.

[47] K. Ninomiya, K. Suzuki, S. Nishimatsu, O. Okada, J. Vac. Sci. Technol. 58 (3) (1985) 1177–1182.

[48] T. Dalton, Unpublished data taken while at Digital Equipment Corporation, Hudson, MA, 1997.

[49] D. Zhang, M.J. Kushner, J. Appl. Phys. 87 (3) (2000) 1060.

[50] X. Li, M. Schaepkens, G.S. Oehrlein, R.E. Ellefson, L.C. Frees, N. Mueller, N. Korner, J. Vac. Sci. Technol. A 17 (5) (1999) 2438.

[51] T.E.F.M. Standaert, M. Schaepkens, N.R. Rueger, P.G.M. Sebel, G.S. Oehrlein, J.M. Cook, J. Vac. Sci. Technol. A 16 (1) (1998) 239.

[52] M. Nakamura, M. Ito, M. Hori, T. Goto, and N. Ishii, Abstracts of Dry Process Symposium, DPS 1999, p 9, November 11–12, 1999 Tokyo, Japan.

[53] J.P. Booth, G. Cunge, P. Chabert, J. Appl. Phys. 85 (6) (1999) 3097–3107.

[54] J. Johannes, E. Meeks, T. Bartel, D.J. Economou, J. Feldsien, T. Dalton, AIAA Conference Proceedings volume, paper AIAA–98–2983 (1998).

[55] N. Mantzaris, E. Gogolides, A. Boudouvis, A. Rhallabi, G. Turban, J. Appl. Phys. 77 (1996) 3718.